I&EC research

Industrial & Engineering Chemistry Research

September 22, 2021

Volume 60, Number 37

pubs.acs.org/IECR

Published by the American Chemical Society for Applied Chemistry and Chemical Engineering

ACS Publications
Most Trusted. Most Cited. Most Read.

www.acs.org

I&EC research
Industrial & Engineering Chemistry Research
pubs.acs.org/IECR
Article

Specific Heat Capacity of Non-Functional and Functional Ionic Liquids during the Absorption of SO_2

Bingru Wang, Long Lin, Shuhang Ren, and Weize Wu*

Cite This: *Ind. Eng. Chem. Res.* 2021, 60, 13740−13747
Read Online

ABSTRACT: Ionic liquids (ILs), a new type of absorbents, are widely used to absorb sulfur dioxide (SO_2) in flue gas. However, the lack of data on the physical properties of ILs has severely hampered their industrial applications. Unlike previous reports on the specific heat capacity of pure ILs, this work not only focuses on measuring the specific heat capacity of pure ILs but also provides the specific heat capacity of IL and SO_2 mixtures during the absorption process. First, we measured the specific heat capacities of six ILs including functional ILs, 1,1,3,3-tetramethylguanidinium lactate ([TMG][Lac]), [TMG][suberate], [TMG][dodecanedioate], and 1-butyl-3-methylimidazolium acetate ([Bmim][Ac]), and non-functional ILs, [TMG][tetrafluoroborate] and [Bmim][tetrafluoroborate], at 303.15−333.15 K. We found that the specific heat capacities of the ILs with or without absorbed SO_2 increase with temperature. The specific heat capacity of ILs increases with the increase of the amount of absorbed SO_2. Then, we investigated the effect of the length of anionic alkyl side chains on the specific heat capacity of SO_2 absorption and found that the specific heat capacity of ILs with shorter alkyl side chains was smaller than that of ILs with longer alkyl side chains. We simulated the absorption process using Gaussian software and found that the specific heat capacities of ILs and SO_2 systems were mainly caused by the vibration of molecules.

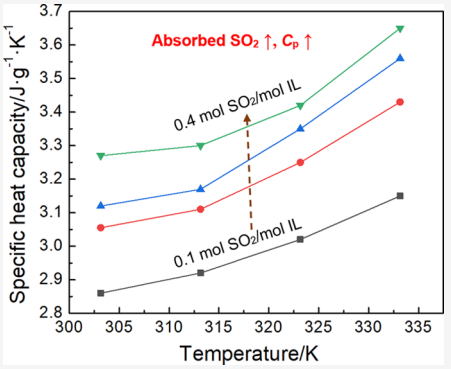

1. INTRODUCTION

Burning fossil fuels is the main method to obtain energy, and sulfur dioxide (SO_2) is released in the burning process. If directly emitted into the atmosphere, SO_2 is harmful to humans and the environment.[1] However, SO_2, when controlled, is an important sulfur resource widely used in the production of pesticides, preservatives, food bleaching, and so forth. To capture and make use of SO_2 released for productive uses, calcium-based and ammonia-based desulfurization methods are most often used. Despite the benefits, these methods have disadvantages such as easy volatilization, blockage of pipes, and high energy consumption.[2]

In recent years, ionic liquids (ILs) have been widely considered as effective solvents for flue gas desulfurization due to their adjustable structures, good physicochemical properties (especially extremely low vapor pressures), and easy recycling.[3,4] Many ILs have been extensively studied in the field of SO_2 absorption. Among them, functional ILs show high potential in the process of SO_2 absorption. However, they are still far from being employed in the industrial application of SO_2 absorption, mainly due to the lack of thermodynamic data on the ILs and on their SO_2 absorption processes.

Specific heat capacity is a very important intrinsic thermodynamic property that can be used to calculate many temperature-dependent physical quantities such as enthalpy, entropy, and Gibbs free energy. It can also be used to calculate the data related to heat exchange in chemical engineering, which facilitate the thermal calculation of equipment and devices. Bendová et al.[5] measured the properties of ILs [C_{16}mim][Cl] and [C_{16}mim][Sac] and found that the specific heat capacities of the ILs increased with their molecular weights. Rotrekl et al.[6] measured the specific heat capacities of [ethoxyC_5im][Tf_2N], [ethoxyiC_5im][Tf_2N], [ethoxycC_5im][Tf_2N], [ethoxy$_3$$C_5$im][$Tf_2N$], and [ethoxyneo$C_5$im][$Tf_2N$] and found that the cyclization of the carbon skeleton led to a reduction in the molecular degrees of freedom compared to the pentyl group. Furthermore, due to the tunable nature of ILs, where anions and cations can produce new ILs in any combination, experimental measurements are not sufficient, so computer technology is needed to predict the specific heat capacity. He et al.[7] developed a QSPR model with temperatures ranging from 191.13 to 550.00 K, taking into account the interaction of anions and cations in ILs. The average absolute relative deviation of the model is 2.5%. Naef[8] developed a molecular volume model and found that the cyclization, branching characteristics, intermolecular hydrogen

Received: June 17, 2021
Published: September 7, 2021

https://doi.org/10.1021/acs.iecr.1c02327
Ind. Eng. Chem. Res. 2021, 60, 13740−13747

bonding, and steric hindrance had an impact on the properties of ILs. The average absolute relative deviation of the model is 2.7%. Rostami et al.[9] employed a hybrid group method of data handling to estimate the specific heat capacity of pure ILs and investigate the effects of the number of methyl groups of the cation and hydrogen atoms of the anion. Their results indicate that the absolute standard deviation is only 1.8%. The above work only measured the specific heat capacities of pure ILs, which do not capture the thermodynamic data of ILs during the absorption process.

In this work, we selected representative functional ILs and nonfunctional ILs and measured their specific heat capacities during the absorption of SO_2. First, we synthesized two functional ILs (1,1,3,3-tetramethylguanidinium lactate—[TMG][Lac] and 1-buty-3-methylimidazolium acetate—[Bmim][Ac]) and two nonfunctional ILs (1,1,3,3-tetramethylguanidinium tetrafluoroborate—[TMG][BF_4] and 1-buty-3-methylimidazolium tetrafluoroborate—[Bmim]-[BF_4]) as they exhibit chemical and physical absorption of SO_2[10] and compared the differences in their specific heat capacities during SO_2 absorption. Then, two functional ILs with different alkyl side chain lengths were synthesized and the effect of alkyl side chain length on specific heat capacity was investigated. Finally, we performed simulations with Gaussian software to illustrate the contribution of molecular vibrations to the specific heat capacity in the system. This paper provides the specific heat capacities of ILs during SO_2 absorption, which is important for the industrial application of ILs for SO_2 capture.

2. EXPERIMENTAL SECTION

2.1. Materials. 1,1,3,3-Tetramethylguanidine (99%) and tetrafluoroboric acid (40%) were obtained from Macklin Biochemical Co., Ltd. (Shanghai, China). Lactic acid (80−85%), [Bmim][BF_4] (99%), and [Bmim][Ac] (99%) were purchased from Sinopharm Chemical Reagent Co., Ltd. (Beijing, China). Octanedioic acid and 1,12-dodecanedioic acid were obtained from Bide Pharmatech Co., Ltd. (Shanghai, China). SO_2 was purchased from Beiwen Gas Manufacturing Factory (Beijing, China). All reagents were used as received.

2.2. Synthesis of ILs. The syntheses of ILs in this experiment follow methods reported in literature.[11−15] For example, [TMG][Lac] was prepared by mixing 1,1,3,3-tetramethylguanidine and lactic acid in a 1:1 molar ratio in an ice-water bath, after which the mixture was stirred for 5 h. The water in the synthesized ILs was removed using rotary evaporators, followed by N_2 bubbling at 80 °C for 24 h. The methods for synthesizing 1,1,3,3-tetramethylguanidinium suberate ([TMG][SUB]), 1,1,3,3-tetramethylguanidinium dodecanedioate ([TMG][DOD]), and [TMG][BF_4] were the same as those reported in the literature.[12−15] Karl-Fischer moisture titration was used to determine the moisture contents of functional ILs. The moisture contents of the synthesized ILs were less than 3%.

2.3. Measurement of Specific Heat Capacities of ILs with Absorbed SO_2. An RC1e calorimeter (Mettler-Toledo, USA) was used to measure the specific heat capacities (C_p) of ILs. The schematic diagram for measuring the specific heat capacities of ILs during the absorption of SO_2 using the RC1e calorimeter is shown in Figure 1. The device is mainly composed of a calorimeter with a cell volume of 80 mL, a controller, and a data acquisition system. The calorimeter used iControl 5.0 software provided by Mettler-Toledo, USA. The heating power of the calorimeter was 2 kW, and the temperatures were controlled with an accuracy of ±0.01 K.

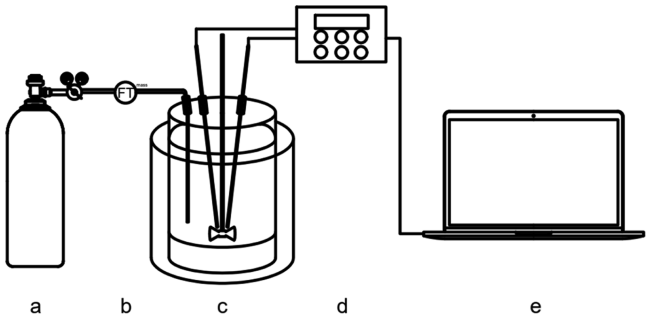

Figure 1. Schematic diagram for measuring the specific heat capacity of ILs during the absorption of SO_2. (a) SO_2 cylinder; (b) mass flow meter; (c) calorimeter; (d) data acquisition system; and (e) computer.

As can be seen from Figure 1, this experiment used the Tr mode to directly control the temperature of the absorbents. The stirring speed in the glass stirrer was initially increased to 200 rpm and then the temperature was increased to the desired one and kept constant. The device was first used to measure the C_p of pure ILs at the beginning. When the C_p measurement of pure ILs was over, pure SO_2 gas was fed into the absorbent in the calorimeter. At the same time, the absorption heat flow curve was measured. A molar ratio of 0.1 mol SO_2 to IL was quantified each time using a calibrated mass flow meter. After the absorption temperature peak returned to its initial value, the next experiment was performed. Finally, the device automatically generated a heat flow curve for the entire absorption process, and the C_p value of the solution after SO_2 absorption was determined.

2.4. Specific Heat Capacity Measurement. The calorimeter had a double-jacketed glass cell as the main component. Both the jacketed temperature T_j of the cell and the temperature T_r of the absorbents could be measured accurately. Then, the heat flow through the cell wall could be calculated using eq 1.

$$Q_c = UA\cdot(T_r - T_j) \tag{1}$$

where Q_c is the heat flow through the cell wall, W; T_r is the temperature of the absorbents, K; U is the heat transfer coefficient, W/(m^2·K); and A is the effective area of the cell, m^2.

The temperature difference is the dynamic heat flow from the cell wall to the absorbents, which is proportional to the temperature difference. The proportionality factor UA was determined by the thermal calibration program.

After the thermal calibration program was finished, the corrected jacket temperature T_a was used instead of T_j because of the effect of the triple thermal resistance of the physical film, oil film, and glass. Therefore, eq 1 can be rewritten as eq 2.

$$Q_c = UA\cdot(T_r - T_a) \tag{2}$$

where T_a is the temperature of the jacket after correction, K.

In the test process of an automatic experimental calorimeter, when the whole system reaches heat flow balance, the heat accumulated in the cell Q_{flow} is equal to the heat flow Q_c, which is shown in eq 3.

$$Q_{flow} = UA\cdot(T_r' - T_a') \tag{3}$$

https://doi.org/10.1021/acs.iecr.1c02327
Ind. Eng. Chem. Res. 2021, 60, 13740−13747

where Q_{flow} is the heat flow through the cell wall, UA is obtained from eq 2, T_r' is the absorption temperature of the absorbent system, and T_a' is the compensation temperature used to maintain a constant temperature.

The heat flow rate in the cell is caused by the absorbents and the temperature sensor and the agitator rotor in the cell, as shown in eq 4.

$$Q_{flow} = \left[\sum_i (m_i \cdot c_{p,i})\right] \cdot \frac{dT_r'}{dt} = (m_r \cdot c_{p,r} + m_i \cdot c_{p,i}) \cdot \frac{dT_r'}{dt} \tag{4}$$

where the subscript r denotes the substance in the cell, subscript i denotes the temperature plug in the cell, $c_{p,r}$ denotes the specific heat capacity of the absorbent in the cell, $c_{p,i}$ denotes the specific heat capacity of the temperature glass plug in the cell, and T_r' denotes the temperature of the absorbent in the cell.

Combining eqs 3 and 4, we derived 5.

$$UA \cdot (T_r' - T_a') = (m_r \cdot c_{p,r} + m_i \cdot c_{p,i}) \cdot \frac{dT_r'}{dt} \tag{5}$$

Among them, the heat transfer coefficient U, the effective area in the cell A, the temperature in the cell T_r', the modified jacket temperature T_a', the mass of the absorbents m_r, the mass of the plug-in in the cell m_j, and the specific heat capacity $c_{p,i}$ are all known values.

The specific heat capacity of the absorbent measured in the cell can be deduced, as shown in eq 6. According to eq 6, the specific heat capacity of the whole absorption system was obtained.

$$c_{p,r} = \left[\frac{UA \cdot (T_r' - T_a')}{\frac{dT_r'}{dt}} - m_i \cdot c_{p,i}\right] \frac{1}{m_r} \tag{6}$$

2.5. Calibration of the Calorimeter. To make the experiment more rigorous, we verified the accuracy of the RC1e calorimeter. The steps of the calibration procedure are shown in Figure S1. Distilled water was chosen as a standard material for this experiment, and the temperature control program was set using iControl software. The accuracy of the instrument was determined by comparing the measured value of specific heat capacity of water under different conditions with the reference value.

2.6. Calibration of the Mass Flow Meter. In order to ensure the accuracy and uniformity of the gas flow of SO_2 in the experiment, we verified the accuracy and reliability of the mass flow meter. A soap film flow meter was used to calibrate the mass flow controller in a laboratory environment at the same temperature and pressure. By calculating the volume of the soap film that moved in a certain time, the flow rate of SO_2 was calculated, which is shown in eq 7.

$$q_{SO_2} = \frac{V_2 - V_1}{t} \tag{7}$$

where q_{SO_2} is the mass flow rate of SO_2 as measured by the soap film flow meter, mL/min; V_1 and V_2 are the volumes of the soap film, mL; and t is the time from scale V_2 to scale V_1, min.

In Table S1, the flow rates displayed by the mass flow meter are compared with the data calculated using eq 7. The displayed data from the mass flow meter were examined three times with a soap film flow meter. As shown in Table S1, the flow rates of the mass flow meter are 60.02, 89.34, and 112.97 mL/min, while the data from the soap film flow meter are 58.20, 88.25, and 113.77 mL/min, respectively, and the absolute relative deviations between them are 3.4, 1.2, and 0.7%, respectively. The absolute deviation is not more than 3.4%. It shows that the mass flow meter can accurately measure the mass flow rate of SO_2 and provide accurate data for the experiment.

2.7. Calculation of Specific Heat Capacities of ILs with Absorbed SO_2. To microscopically explain the variation of the specific heat capacity of the system during the absorption of SO_2 with the ILs, the absorption process was simulated using Gaussian software.[16] The ILs and SO_2 molecules are composed of four elements, C, H, O and S, all of which belong to the first four periods of the periodic table, and the relativistic effect is not obvious. Therefore, the use of superfluous potential basis groups was not considered. In this work, we optimized the molecular structures and made the analysis on the vibrational frequencies. Considering the accuracy and efficiency of the calculation, we first used Gaussian software[16] and chose the DFT calculation method, 6-31G++(d,p). The optimization of the geometric structure of ILs and SO_2 molecules was made for the base group, and the specific heat capacity in the output file was extracted using Shermo software.[17] Different temperatures were set to predict the specific heat capacity of the ILs. The specific heat capacity of the ILs was then extracted from the output file using Shermo software and set at temperatures of 313.15, 323.15, 333.15, and 343.15 K to predict the specific heat capacity.

2.8. Error Analysis. On the basis of eq 6, the uncertainties of measured $C_{p,r}$ were estimated using eq 8.

$$\begin{aligned}\frac{\Delta c_{p,r}}{c_{p,r}} &= \left|\frac{\partial \ln c_{p,r}}{\partial U}\right| \Delta U + \left|\frac{\partial \ln c_{p,r}}{\partial A}\right| \Delta A + \left|\frac{\partial \ln c_{p,r}}{\partial T_r'}\right| \frac{\Delta T_r'}{T_r'} \\ &+ \left|\frac{\partial \ln c_{p,r}}{\partial T_a'}\right| \frac{\Delta T_a'}{T_a'} + \left|\frac{\partial \ln c_{p,r}}{\partial \frac{dT_r'}{dt}}\right| \frac{\Delta T_r'}{\Delta t} \\ &+ \left|\frac{\partial \ln c_{p,r}}{\partial m_r}\right| \Delta m_r \\ &= \left|\frac{\Delta U}{U}\right| + \left|\frac{\Delta A}{A}\right| + \left|\frac{\frac{\Delta T_r'}{T_r'}}{1 - \frac{\Delta T_r'}{T_r'}}\right| + \left|\frac{\frac{\Delta T_a'}{T_a'}}{1 - \frac{\Delta T_a'}{T_a'}}\right| \\ &+ \left|\frac{\Delta T_r'}{\Delta t}\right| + \left|\frac{\Delta m_r}{m_r}\right|\end{aligned} \tag{8}$$

where $\Delta U = 0.001$, $\Delta A = 0.01$, and $\Delta m_r = 0.001$, and the relative deviations of heat flow at different temperatures are listed in Table S2. The estimated uncertainties for each data point are listed in the data tables.

3. RESULTS AND DISCUSSION

3.1. Verification of the Accuracy of the RC1e Calorimeter. To ensure the accuracy of the data measured by the RC1e calorimeter, the specific heat capacities of water at different temperatures were measured with this device and compared with the data from the NIST database. As shown in Table 1, the specific heat capacities measured by the RC1e at 310.53, 340.11, 344.95, and 359.49 K are 4.176, 4.185, 4.116,

https://doi.org/10.1021/acs.iecr.1c02327
Ind. Eng. Chem. Res. 2021, 60, 13740−13747

Table 1. Comparison of the Specific Heat Capacity of Water from This Work with Those from Literature

temperature (K)	C_p of water from this work ($J \cdot g^{-1} \cdot K^{-1}$)	C_p of water from NIST ($J \cdot g^{-1} \cdot K^{-1}$)	ARD %
310.53	4.176	4.174	0.11
340.11	4.185	4.184	0.04
344.95	4.116	4.188	1.72
359.49	4.205	4.202	0.08

and 4.305 $J \cdot g^{-1} \cdot K^{-1}$, respectively, while the specific heat capacities from the NIST data are 4.174, 4.185, 4.188, and 4.203 $J \cdot g^{-1} \cdot K^{-1}$, respectively.[18] Compared with the data from NIST, the relative deviation of this work does not exceed 1.72%. In all, the automated calorimeter used in this work is accurate for measuring the specific heat capacity of the ILs.

3.2. Specific Heat Capacity of Pure ILs. First, the specific heat capacities of six pure ILs, [TMG][Lac], [TMG][BF_4], [TMG][SUB], [TMG][DOD], [Bmim][Ac] and [Bmim][BF_4], were measured at temperatures from 303.15 to 333.15 K. The detailed data of specific heat capacities of six pure ILs are shown in Table S3. Figure 2 illustrates the specific heat capacities of six pure ILs as a function of temperature. It can be seen from the figure that the specific heat capacities of all six ILs increase with increasing temperature. For example, the specific heat capacity of [TMG][Lac] increases from 3.132 to 3.433 $J \cdot g^{-1} \cdot K^{-1}$ when the temperature increases from 303.15 to 353.15 K.

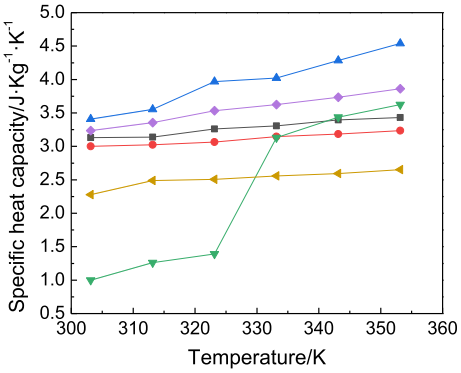

Figure 2. Specific heat capacity of six kinds of pure ILs ([TMG][Lac], [TMG][BF_4], [TMG][SUB], [TMG][DOD], [Bmim][Ac], and [Bmim][BF_4]) as a function of temperature. ■ black, [TMG][Lac]; ● red, [TMG][BF_4]; ▲ blue, [TMG][SUB]; ▼ green, [TMG][DOD]; ◆ violet, [Bmim][Ac]; and ◀ yellow, [Bmim][BF_4].

It can be clearly seen from Figure 2 that at low temperatures of 303.15, 313.15, and 323.15 K, the specific heat capacity of [TMG][DOD] is significantly small. In contrast, at high temperatures of 333.15, 343.15, and 353.15 K, the specific heat capacity of [TMG][DOD] is significantly large. The reason is that at lower temperatures, [TMG][DOD] appears as a solid, and the specific heat capacity of the solid state of the same substance is significantly lower than that of the liquid. Therefore, the phase transition of [TMG][DOD] between 323.15 and 333.15 K leads to a significant change in the curve.

3.3. Effects of Temperature and SO_2 Absorption Amount on Specific Heat Capacity. The specific heat capacity data of [TMG][Lac] and [TMG][BF_4] with the same cation of $[TMG]^+$ after absorbing the same amount of SO_2 at different temperatures are shown in Table S4, which are illustrated in Figure 3A,B for comparison. It is easy to see that their specific heat capacities increase with the increase of temperature for the same amount of absorbed SO_2. For example, the specific heat capacity of [TMG][Lac] increases from 3.607 to 4.098 $J \cdot g^{-1} \cdot K^{-1}$ when the temperature increases from 303.15 to 333.15 K at an absorption of 0.200 mol SO_2/mol IL. In addition, it can be seen that their specific heat capacities increase with the increase of SO_2 absorption amount at the same temperature. For example, at the temperature of 333.15 K, the specific heat capacity of [TMG][BF_4] increases from 2.705 to 4.763 $J \cdot g^{-1} \cdot K^{-1}$ when the SO_2 absorption amount is increased from 0.100 to 0.400 mol SO_2/mol IL. The specific heat capacity of [TMG][Lac] is greater than that of [TMG][BF_4] at the same temperature with the same amount of SO_2 absorption. For example, at a temperature of 313.15 K for a SO_2 absorption amount of 0.300 mol SO_2/mol IL, the specific heat capacity of [TMG][Lac] is 3.754 $J \cdot g^{-1} \cdot K^{-1}$, which is significantly larger than that of [TMG][BF_4], 3.147 $J \cdot g^{-1} \cdot K^{-1}$.

As we know, specific heat capacity is an inherent property of a substance and is related to the substance itself. There are three modes of molecular motions in a substance: translation, rotation, and vibration. The amplitudes of translation, rotation, and vibration determine the specific heat capacity of a substance. When the temperature increases, the amplitudes of translation, rotation, and vibration of the molecules increase, resulting in an increase in the specific heat capacity of the substance. Moreover, at an identical condition, a larger amount of SO_2 absorption in the solution can result in an increase in the overall specific heat capacity of the solution. After the absorption of SO_2 in the absorbent system, the number of atoms in the system is increased, which enhances the amplitude of vibration, and then the specific heat capacity of the system.

The reasons for the difference in specific heat capacities of the two ILs, [TMG][Lac] and [TMG][BF_4], are shown as follows. The two ILs have different anions. The anion of [TMG][Lac] is lactate, accounting for a functional IL, while the anion of [TMG][BF_4] is tetrafluoroborate, accounting for a non-functional IL.[10] The absorption mechanism by the two ILs is different.[12] The functionalized IL [TMG][Lac] mainly relies on a chemical interaction in the absorption process and has a higher impact on the specific heat capacity of the absorbent system. In contrast, the non-functionalized IL [TMG][BF_4] mainly relies on the physical interaction in the absorption process and dissolves SO_2 molecules physically. Hence, [TMG][BF_4] has a lower impact on the specific heat capacity of the absorbent system.

The specific heat capacity data of [Bmim][Ac] and [Bmim][BF_4] with the same cation $[Bmim]^+$ after absorbing different amounts of SO_2 at different temperatures are also shown in Table S4 for comparison. Figure 3C,D illustrates the specific heat capacity of the above two ILs with the same cation as a function of temperature. It is easy to see that the specific heat capacities of both ILs increase with increasing temperature at the same amount of SO_2 absorption. For example, at an absorption amount of 0.100 mol SO_2/mol IL, the specific heat capacity of [Bmim][Ac] increases from 2.862 to 3.152 $J \cdot g^{-1} \cdot K^{-1}$ when the temperature increases from 303.15 to 333.15 K. At the same SO_2 absorption amount, the specific heat capacity of [Bmim][BF_4] increases from 2.199 to 3.001 $J \cdot g^{-1} \cdot K^{-1}$ when the temperature increases from 303.15 to 333.15 K. At the same temperature, their specific heat capacities

https://doi.org/10.1021/acs.iecr.1c02327
Ind. Eng. Chem. Res. 2021, 60, 13740−13747

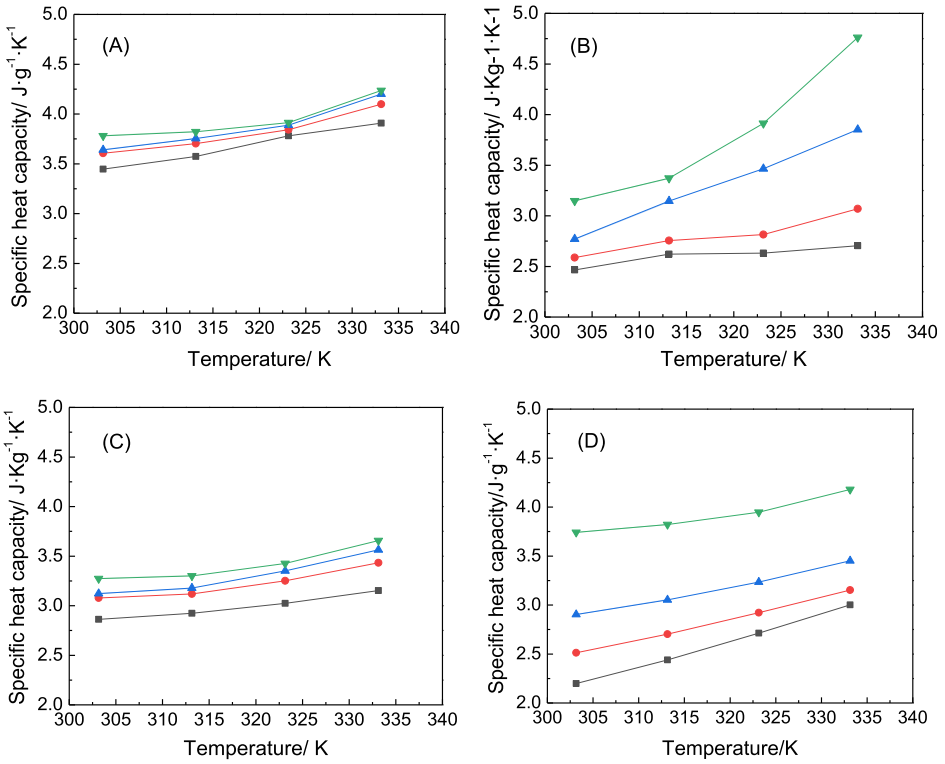

Figure 3. Specific heat capacity data of four kinds of ILs as a function of temperature after absorbing different amounts of SO_2. ■ black, 0.100 mol SO_2/mol IL; ● red, 0.200 mol SO_2/mol IL; ▲ blue, 0.300 mol SO_2/mol IL; and ▼ green, 0.400 mol SO_2/mol IL; (A) [TMG][Lac]; (B) [TMG][BF_4]; (C) [Bmim][Ac]; and (D) [Bmim][BF_4].

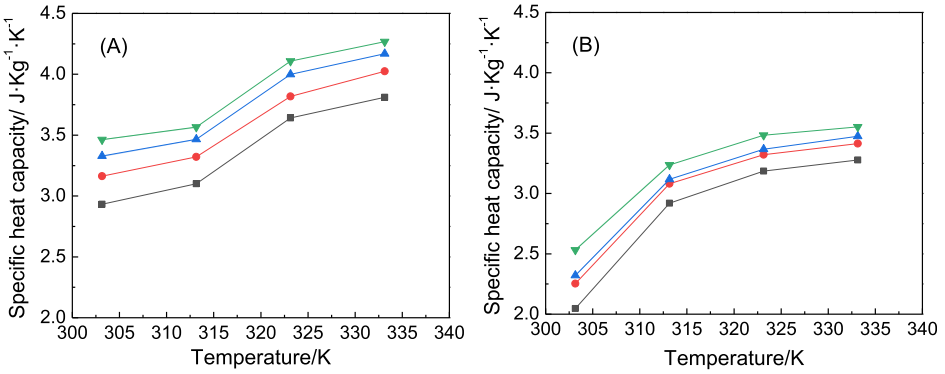

Figure 4. Specific heat capacity data of two kinds of ILs after absorbing the same amount of SO_2 at different temperatures and different amounts of absorbed SO_2. ■ black, 0.100 mol SO_2/mol IL; ● red, 0.200 mol SO_2/mol IL; ▲ blue, 0.300 mol SO_2/mol IL; and ▼ green, 0.400 mol SO_2/mol IL. (A) [TMG][DOD] and (B) [TMG][SUB].

increase with increasing amount of absorbed SO_2. For example, at the temperature of 323.15 K, the specific heat capacity of [Bmim][Ac] increases from 3.025 to 3.427 J·g^{-1}·K^{-1} when the absorption of SO_2 increases from 0.100 to 0.400 mol SO_2/mol IL. In contrast, at the same temperature, the specific heat capacity of [Bmim][BF_4] increases from 2.712 to 3.948 J·g^{-1}·K^{-1} when the absorption of SO_2 increases from 0.100 to 0.400 mol SO_2/mol IL. The specific heat capacity of [Bmim][Ac] is larger than that of [Bmim][BF_4] at the same temperature and the same amount of absorbed SO_2. The reasons for the difference in specific heat capacities of [Bmim][Ac] and [Bmim][BF_4] by temperature and SO_2 absorption amount are similar to those of [TMG][Lac] and [TMG][BF_4].

Note that for functional ILs [TMG][Lac] and [Bmim][Ac], SO_2 absorption amount has a smaller influence on the specific heat capacities than those for non-functional ILs [TMG][BF_4] and [Bmim][BF_4], as shown in Figure 3A–D. For instance, at a temperature of 303.15 K, when the absorption of SO_2 increases from 0.100 to 0.400 mol SO_2/mol IL, the specific heat capacity of [TMG][Lac] is increased by 9.7%, but that of [TMG][BF_4] is increased by 27.8%; the specific heat capacity of [Bmim][Ac] is increased by 14.4%, but that of [Bmim]-[BF_4] is increased by 70.2%. The reason may result from the higher interaction of functional ILs with SO_2 (chemical interaction) than that of non-functional ILs (physical interaction).

3.4. Influence of the Anionic Side Chain Alkyl Length of ILs on Their Specific Heat Capacities. In order to further investigate the effect of side chains of the anion of functional ILs on their specific heat capacities, [TMG][SUB]

https://doi.org/10.1021/acs.iecr.1c02327
Ind. Eng. Chem. Res. 2021, 60, 13740−13747

and [TMG][DOD] with the same cation were synthesized, and the specific heat capacities of the two ILs with different SO_2 absorption amounts at different temperatures were measured. Table S5 shows the specific heat capacity data of [TMG][SUB] and [TMG][DOD] after absorbing SO_2 at different temperatures. The specific heat capacities of the two ILs are illustrated in Figure 4. It can be seen that the specific heat capacities of both ILs increase with the increase of temperature at the same amount of SO_2 absorption. For example, at an absorption amount of 0.100 mol SO_2/mol IL, the specific heat capacity of [TMG][DOD] increases from 2.932 to 3.810 $J·g^{-1}·K^{-1}$ when the temperature increases from 303.15 to 333.15 K. At the same absorption, the specific heat capacity of [TMG][SUB] increases from 2.046 to 3.278 $J·g^{-1}·K^{-1}$ when the temperature increases from 303.15 to 333.15 K.

At the same temperature, the specific heat capacity of both ILs increases with the increase of SO_2 absorption amount. For example, at a temperature of 313.15 K, the specific heat capacity of [TMG][DOD] increases from 3.100 to 3.567 $J·g^{-1}·K^{-1}$ when the absorption amount of SO_2 increases from 0.100 to 0.400 mol SO_2/mol IL. At the same temperature, the specific heat capacity of [TMG][SUB] increases from 2.920 to 3.237 $J·g^{-1}·K^{-1}$ when the absorption amount of SO_2 increases from 0.100 to 0.400 mol SO_2/mol IL.

At the same amount of SO_2 absorption, the internal energy of the IL + SO_2 system gradually increases with the increase of temperature, and more molecules reach the activated state. Therefore, with the increase of temperature, the specific heat capacity increases. The increase in the SO_2 absorption amount leads to an increase in the specific heat capacity of the IL after absorbing SO_2.

As shown in Table S5, the specific heat capacity of [TMG][DOD] is larger than that of [TMG][SUB] at the same temperature and the same amount of SO_2 absorption. The two dicarboxylate-based ILs are functionalized ones,[10] but they are different in the length of the anionic alkyl chains. The alkyl chain of [TMG][DOD] is significantly longer than that of [TMG][SUB]. The different lengths of the alkyl chains can result in different symmetries of the two ILs. The longer anionic alkyl chain of [TMG][DOD] has a poorer symmetry, while the shorter alkyl chain [TMG][SUB] has a much better symmetry. Moreover, [TMG][DOD] has a longer anionic alkyl chain and then has a higher amplitude of vibration in its inner molecules, resulting higher specific heat capacity than [TMG][SUB]. Therefore, the specific heat capacity of [TMG][SUB] is smaller than that of [TMG][DOD] when the same amount of SO_2 is absorbed at the same temperature.

3.5. Simulation Calculations of Specific Heat Capacity. The absorption process of SO_2 with four [TMG]-based ILs, [TMG][Lac], [TMG][SUB], [TMG][DOD], and [TMG][BF_4], was simulated to investigate the specific heat capacities of the ILs during SO_2 absorption. The specific heat capacity of the IL was then extracted from the output file using Shermo software and set at temperatures of 313.15, 323.15, 333.15, and 343.15 K to predict the specific heat capacity.

Figure 5 shows the optimized structures of the four ILs, as well as their structures, after binding to SO_2 molecules. Three ILs, [TMG][Lac], [TMG][SUB], and [TMG][DOD], contain carboxyl groups. Figure 5b,d,f shows that all the SO_2 molecules interact with the carboxyl groups on the anion of the three ILs. The corresponding S···O bond lengths are 1.337 ,1.773, and 1.842 Å for the interaction of SO_2 with [TMG][Lac], [TMG][SUB], and [TMG][DOD], respectively. Figure 5d

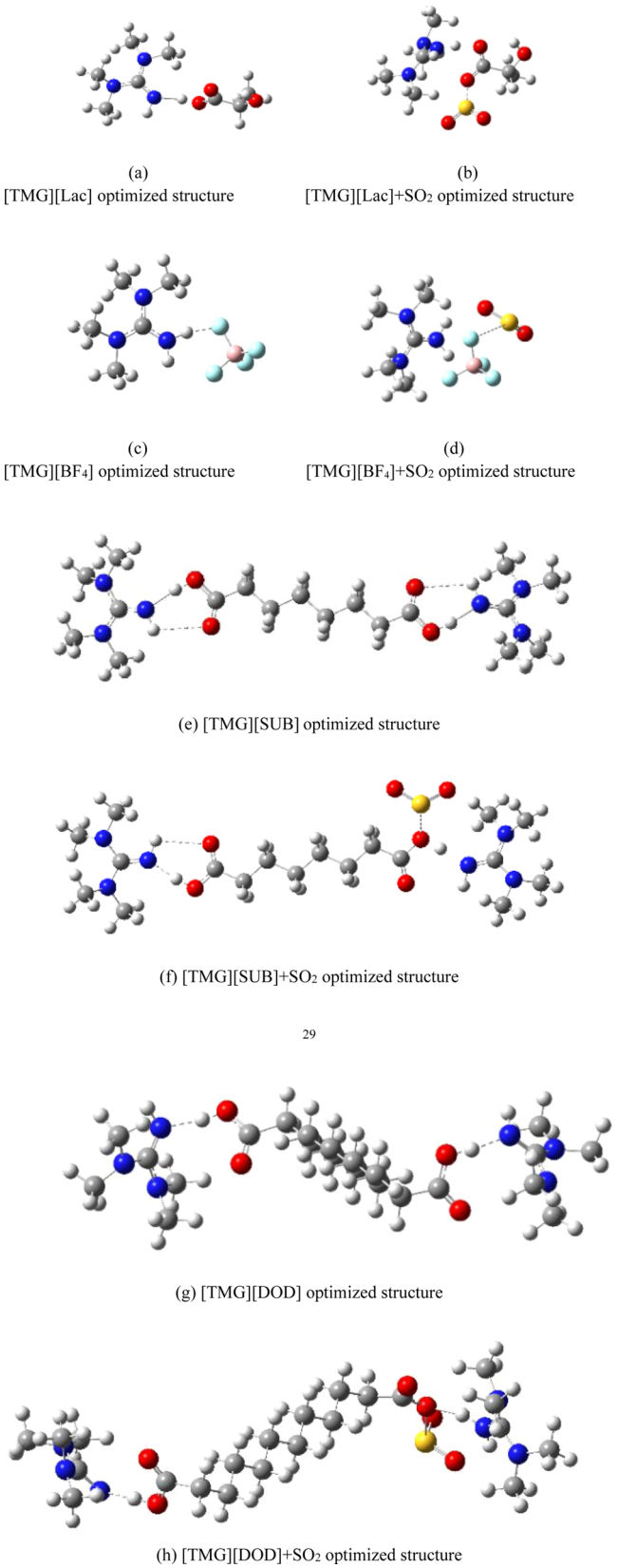

Figure 5. Structural optimization of ILs before and after SO_2 absorption. (a) [TMG][Lac] optimized structure, (b) [TMG][Lac] + SO_2 optimized structure, (c) [TMG][BF_4] optimized structure, (d) [TMG][BF_4] + SO_2 optimized structure, (e) [TMG][SUB] optimized structure, (f) [TMG][SUB] + SO_2 optimized structure, (g) [TMG][DOD] optimized structure, and (h) [TMG][DOD] + SO_2 optimized structure.

https://doi.org/10.1021/acs.iecr.1c02327
Ind. Eng. Chem. Res. 2021, 60, 13740−13747

shows that the SO_2 molecule interacts with the BF_4^- anion. After obtaining these optimized structures, the wave function file generated by the calculation was further imported into Shermo software to simulate the changes in the overall specific heat capacity of the system when different ILs absorbed sulfur dioxide.

Table 2 shows the calculated specific heat capacities of the four ILs [TMG][Lac], [TMG][BF_4], [TMG][SUB], and [TMG][DOD] before and after SO_2 absorption at different temperatures. Note that all calculations were assumed as an ideal gas, and the amount of IL substance was 1 mol. From Table 2, it can be seen that the specific heat capacity of ILs increases with increasing temperature before the absorption of SO_2. After the absorption of SO_2, the specific heat capacity of the absorbed product (IL + SO_2) also increases with the increase of temperature. The specific heat capacities were contributed by molecular translation, molecular rotation, and intramolecular vibration. Molecular translation and molecular rotation were found to be constant, 0.205 and 0.123 $J{\cdot}g^{-1}{\cdot}K^{-1}$, respectively. In particular, the contribution of the molecular charge to the specific heat capacity, $C_{p,ele}$, is 0. The increase of temperature only affects the specific heat capacity contributed by intramolecular vibrations. For example, as for [TMG][Lac] IL, when the temperature is increased from 313.15 to 333.15 K, the specific heat capacity contributed by intramolecular vibrations increases from 2.436 to 2.563 $J{\cdot}g^{-1}{\cdot}K^{-1}$. The specific heat capacity of a substance is an intrinsic property that refers to the "capacity" of a substance to absorb energy as its temperature changes. At the macroscopic level, the absorbed energy is reflected in the change of the internal energy of the substance. At the microscopic level, the change in the internal energy of a substance is related to the way of atoms within a molecule and the molecule as a whole vibration. Thus, through the change in internal energy, it is possible to establish a relationship between specific heat capacity and microscopic properties. The specific heat capacity is linked to the microscopic properties of a substance through the intermediate quantity of internal energy. In statistical thermodynamics, the thermochemical quantity can be approximated as the sum of the contributions of translational, rotational, vibrational, and electronic energies. Therefore, for the specific heat capacity of ILs, the overall specific heat capacity, $C_{p,total}$, is the sum of these four components, $C_{p,trans}$, $C_{p,rot}$, $C_{p,vib}$, and $C_{p,ele}$, which is shown in eq 9.

$$c_{p,total} = c_{p,trans} + c_{p,rot} + c_{p,vib} + c_{p,ele} \quad (9)$$

Based on the ideal gas assumption, the contribution of the overall molecular advection to the constant pressure specific heat capacity, $C_{p,trans}$ is obtained as the contribution to the constant volume heat capacity $C_{V,trans}$ in this case, where $C_{V,trans}$ is equal to 1.5 times the ideal gas constant.[19,20] Accordingly, the change in temperature does not affect $C_{V,trans}$. Hence, the values of $C_{V,trans}$ are constant. Therefore, the $C_{p,trans}$ generated by the molecular translation is constant, and the $C_{p,trans}$ in Table 2 is 0.205 $J{\cdot}g^{-1}{\cdot}K^{-1}$.

The rotation of molecules also contributes to the thermodynamic quantities of ILs, and when the molecules are linear, $C_{P,rot,lin}$ is equal to the ideal gas constant. When the molecule is nonlinear, the $C_{P,rot,nonlin}$ is equal to 1.5 times that of the ideal gas constant. For ILs, which are nonlinear molecules, it is appropriate to use the equation to calculate $C_{P,rot,nonlin}$, which shows that there is no temperature-dependent physical quantity. In this case, the change in the temperature does not affect the value of $C_{P,rot,nonlin}$. Therefore, the $C_{P,rot,nonlin}$ generated by the rotation of molecules is a constant. That is, the $C_{P,rot,nonlin}$ in Table 2 is 0.123 $J{\cdot}g^{-1}{\cdot}K^{-1}$.

There are various modes of vibration of molecules, and according to the knowledge of statistical thermodynamics, the mode of vibration of each molecule can be described by a partition function. The thermodynamic quantities caused by different forms of vibrations can be written as the sum of the respective contributions of each vibration mode. The temperature is related to the contribution of molecular vibrations to the heat capacity, $C_{P,vib}$.

The contribution of electron excitation to the specific heat capacity data comes from two components, that is, electron energy and electron excitation. At room temperature, only states with excitation energies less than a few tenths of an eV contribute significantly to the thermodynamic data, so the contribution of electron excitation is usually not considered.[19,20] Therefore, the contribution of electron excitation to specific heat capacity, $C_{p,ele}$, is 0, as shown in Table 2.

Table 2. Comparison of the Specific Heat Capacity of Different ILs before and after Absorbing SO_2 by Simulation Calculations[a]

ILs	temp./K	$c_{p,trans}$	$c_{p,rot}$	$c_{p,vib}$	$c_{p,ele}$	$c_{p,total}$
[TMG][BF_4]	313.15	0.205	0.123	2.194	0	2.522
	323.15	0.205	0.123	2.248	0	2.575
	333.15	0.205	0.123	2.300	0	2.628
[TMG][BF_4] + SO_2	313.15	0.205	0.123	2.096	0	2.345
	323.15	0.205	0.123	2.139	0	2.388
	333.15	0.205	0.123	2.183	0	2.432
[TMG][Lac]	313.15	0.205	0.123	2.436	0	2.759
	323.15	0.205	0.123	2.499	0	2.824
	333.15	0.205	0.123	2.563	0	2.887
[TMG][Lac] + SO_2	313.15	0.205	0.123	2.630	0	2.877
	323.15	0.205	0.123	2.686	0	2.933
	333.15	0.205	0.123	2.742	0	2.989
[TMG][SUB]	313.15	0.205	0.123	3.687	0	3.917
	323.15	0.205	0.123	3.782	0	4.012
	333.15	0.205	0.123	3.877	0	4.107
[TMG][SUB] + SO_2	313.15	0.205	0.123	3.337	0	3.578
	323.15	0.205	0.123	3.417	0	3.658
	333.15	0.205	0.123	3.498	0	3.739
[TMG][DOD]	313.15	0.205	0.123	3.502	0	3.829
	323.15	0.205	0.123	3.590	0	3.918
	333.15	0.205	0.123	3.684	0	4.011
[TMG][DOD] + SO_2	313.15	0.205	0.123	3.772	0	4.099
	323.15	0.205	0.123	3.865	0	4.193
	333.15	0.205	0.123	3.961	0	4.289

[a]Unit: $J{\cdot}g^{-1}{\cdot}K^{-1}$.

4. CONCLUSIONS

This work complements the specific heat capacity data of several ILs during the absorption process of varying amounts of SO_2. The specific heat capacities of six pure ILs and six ILs after the absorption of SO_2 amounts of 0.100, 0.200, 0.300, and 0.400 mol SO_2/mol IL were measured at 303.15, 313.15, 323.15, and 333.15 K. The results indicate that the specific heat capacities of six pure ILs with or without absorbed SO_2 increase with increasing temperature. The specific heat

https://doi.org/10.1021/acs.iecr.1c02327
Ind. Eng. Chem. Res. 2021, 60, 13740−13747

capacities of six ILs increase with increasing amounts of absorbed SO_2. The specific heat capacity of ILs increases with the growth of the carbon chain of the anion. This work also simulated the change of specific heat capacity of the overall system when SO_2 was absorbed by different ILs through software. The trends of the specific heat capacity of ILs with and without absorbed SO_2 are similar to those of experiment, and the specific heat capacities of ILs with and without absorbed SO_2 are mainly caused by the vibration of molecules.

■ ASSOCIATED CONTENT

Supporting Information

The Supporting Information is available free of charge at https://pubs.acs.org/doi/10.1021/acs.iecr.1c02327.

Steps of the calibration procedure; comparison of SO_2 flow rates; relative deviation of heat flow at different temperatures; and specific heat capacity of pure ILs and after absorbing SO_2 at different temperatures (PDF)

■ AUTHOR INFORMATION

Corresponding Author

Weize Wu − *State Key Laboratory of Chemical Resource Engineering, College of Chemical Engineering, Beijing University of Chemical Technology, Beijing 100029, China;* orcid.org/0000-0002-0843-3359; Phone: +86 10 64427603; Email: wzwu@mail.buct.edu.cn; Fax: +86 10 64427603

Authors

Bingru Wang − *State Key Laboratory of Chemical Resource Engineering, College of Chemical Engineering, Beijing University of Chemical Technology, Beijing 100029, China*

Long Lin − *State Key Laboratory of Chemical Resource Engineering, College of Chemical Engineering, Beijing University of Chemical Technology, Beijing 100029, China*

Shuhang Ren − *State Key Laboratory of Chemical Resource Engineering, College of Chemical Engineering, Beijing University of Chemical Technology, Beijing 100029, China;* orcid.org/0000-0003-3253-8852

Complete contact information is available at: https://pubs.acs.org/10.1021/acs.iecr.1c02327

Funding

This project was supported financially by the National Natural Science Foundation of China (no. 21176020 and 21306007). The authors also thank the Long-Term Subsidy Mechanism from the Ministry of Finance and the Ministry of Education of PRC (BUCT).

Notes

The authors declare no competing financial interest.

■ REFERENCES

(1) Smith, S. J.; van Aardenne, J.; Klimont, Z.; Andres, R. J.; Volke, A.; Delgado Arias, S. Anthropogenic Sulfur Dioxide Emissions: 1850−2005. *Atmos. Chem. Phys.* **2011**, *11*, 1101−1116.

(2) Soud, H. N.; Research, I. C. *Developments in FGD*; IEA Coal Research, 2000; Vol. 29.

(3) Ren, S.; Hou, Y.; Zhang, K.; Wu, W. Ionic Liquids: Functionalization and Absorption of SO_2. *Green Energy Environ.* **2018**, *3*, 179−190.

(4) Sun, Y.; Ren, S.; Hou, Y.; Zhang, K.; Zhang, Q.; Wu, W. Highly Reversible and Efficient Absorption of Low-Concentration no by Amino-Acid-Based Ionic Liquids. *ACS Sustainable Chem. Eng.* **2020**, *8*, 3283−3290.

(5) Bendová, M.; Wagner, Z.; Bogdanov, M. G.; Čanji, M.; Zdolšek, N. Heat Capacity of 1-Hexadecyl-3-Methylimidazolium based Ionic Liquids in Solid and Liquid Phase. *J. Mol. Liq.* **2020**, *305*, 112847.

(6) Rotrekl, J.; Jandová, V.; Storch, J.; Velíšek, P.; Cuřínová, P.; Schwarz, J.; Wagner, Z.; Bendová, M. Thermal Properties of Novel Oligoether-Substituted Ionic Liquids and the Influence of Alkyl-Substituent Isomery. *Fluid Phase Equilib.* **2020**, *514*, 112561.

(7) He, W.; Yan, F.; Jia, Q.; Xia, S.; Wang, Q. Prediction of Ionic Liquids Heat Capacity at Variable Temperatures based on the Norm Indexes. *Fluid Phase Equilib.* **2019**, *500*, 112260.

(8) Naef, R. Calculation of the Isobaric Heat Capacities of the Liquid and Solid Phase of Organic Compounds at and around 298.15 K Based on Their "True" Molecular Volume. *Molecules* **2019**, *24*, 1626.

(9) Rostami, A.; Hemmati-Sarapardeh, A.; Karkevandi-Talkhooncheh, A.; Husein, M. M.; Shamshirband, S.; Rabczuk, T. Modeling Heat Capacity of Ionic Liquids Using Group Method of Data Handling: A Hybrid and Structure-Based Approach. *Int. J. Heat Mass Transfer* **2019**, *129*, 7−17.

(10) Ren, S.; Hou, Y.; Tian, S.; Chen, X.; Wu, W. What Are Functional Ionic Liquids for the Absorption of Acidic Gases? *J. Phys. Chem. B* **2013**, *117*, 2482−2486.

(11) Zhang, K.; Li, H.; Ren, S.; Wu, W.; Bao, Y. Specific Heat Capacities of Two Functional Ionic Liquids and Two Functional Deep Eutectic Solvents for the Absorption of SO_2. *J. Chem. Eng. Data* **2017**, *62*, 2708−2712.

(12) Huang, J.; Riisager, A.; Wasserscheid, P.; Fehrmann, R. Reversible Physical Absorption of SO_2 by Ionic Liquids. *Chem. Commun.* **2006**, *42*, 4027−4029.

(13) Meng, X.; Wang, J.; Jiang, H.; Zhang, X.; Liu, S.; Hu, Y. Guanidinium-Based Dicarboxylic Acid Ionic Liquids for SO_2 Capture. *J. Chem. Technol. Biotechnol.* **2017**, *92*, 767−774.

(14) Meng, X.; Wang, J.; Xie, P.; Jiang, H.; Hu, Y.; Chang, T. Structure and SO_2 Absorption Properties of Guanidinium-Based Dicarboxylic Acid Ionic Liquids. *Energy Fuels* **2018**, *32*, 1956−1962.

(15) Wu, W.; Han, B.; Gao, H.; Liu, Z.; Jiang, T.; Huang, J. Desulfurization of Flue Gas: SO_2 Absorption by an Ionic Liquid. *Angew. Chem., Int. Ed.* **2004**, *43*, 2415−2417.

(16) Frisch, M. J.; Trucks, G. W.; Schlegel, H. B.; Scuseria, G. E.; Robb, M. A.; Cheeseman, J. R.; Scalmani, G.; Barone, V.; Petersson, G. A.; Nakatsuji, H.; Li, X.; Caricato, M.; Marenich, A.; Bloino, J.; Janesko, B. G.; Gomperts, R.; Mennucci, B.; Hratchian, H. P.; Ortiz, J. V.; Izmaylov, A. F.; Sonnenberg, J. L.; Williams-Young, D.; Ding, F.; Lipparini, F.; Egidi, F.; Goings, J.; Peng, B.; Petrone, A.; Henderson, T.; Ranasinghe, D.; Zakrzewski, V. G.; Gao, J.; Rega, N.; Zheng, G.; Liang, W.; Hada, M.; Ehara, M.; Toyota, K.; Fukuda, R.; Hasegawa, J.; Ishida, M.; Nakajima, T.; Honda, Y.; Kitao, O.; Nakai, H.; Vreven, T.; Throssell, K.; Montgomery, J. A., Jr.; Peralta, J. E.; Ogliaro, F.; Bearpark, M.; Heyd, J. J.; Brothers, E.; Kudin, K. N.; Staroverov, V. N.; Keith, T.; Kobayashi, R.; Normand, J.; Raghavachari, K.; Rendell, A.; Burant, J. C.; Iyengar, S. S.; Tomasi, J.; Cossi, M.; Millam, J. M.; Klene, M.; Adamo, C.; Cammi, R.; Ochterski, J. W.; Martin, R. L.; Morokuma, K.; Farkas, O.; Foresman, J. B.; Fox, D. J. *Gaussian 09*, Revision D.01: Wallingford, CT, 2016.

(17) Lu, T.; Chen, Q. Shermo: A General Code for Calculating Molecular Thermochemistry Properties. *Comput. Theor. Chem.* **2021**, *1200*, 113249.

(18) Linstrom, P. J.; Mallard, W. G. *NIST Chemistry WebBook, NIST Standard Reference Database Number 69*; National Institute of Standards and Technology: Gaithersburg MD, 20899, 2021. (retrieved June 8, 2021).

(19) Jensen, F. *Introduction to Computational Chemistry*; John Wiley & Sons, 2017.

(20) Irikura, K. K. *Essential Statistical Thermodynamics, Computational Thermochemistry, Appendix B*; American Chemical Society, 1998.